Coupling subdomains with heterogeneous time integrators and incompatible time steps

Najib Mahjoubi, Anthony Gravouil, Alain Combescure

Coupling subdomains with heterogeneous time integrators and incompatible time steps

Najib Mahjoubi · Anthony Gravouil · Alain Combescure

Abstract The work presented in this publication can be categorized among domain decomposition methods of the dual Schur type applied to structural dynamics. This approach leads to lower CPU times and better control of the accuracy of the time discretization and allows to take into account multi-time-scale effects which arise in transient structural dynamics. In order to consider incompatible time scales, one has to enforce continuity at the interfaces between the subdomains. Here, we propose a general formalism which enables the coupling of subdomains with their own numerical time integration scheme. The proposed method enables one to take into account possible nonlinearities which may present different time scale between the subdomains in a general manner for a wide range of time numerical scheme. This method also offers an important improvement for industrial software with easy implementation. Linear and nonlinear numerical examples are proposed in order to show the efficiency and the robustness of the method.

Keywords Subdomain methods · Multi-time-scale · Heterogeneous time integrators · Incompatible time scales

1 Introduction

Nonlinear transient dynamic structural calculations are often very expensive in CPU time as well as in memory size. In many applications, some regions must be very finely meshed in time to ensure good-quality local prediction, while in other regions this degree of refinement is unnecessary. In explicit nonlinear dynamics problems, the smallest mesh size determines the time step for the whole domain. Therefore, many useless calculations end up being performed on the coarse part of the mesh. In a more general point of view, it should be interesting to define incompatible meshes in the various parts of the structure and not have to worry about mesh size and time step compatibility at the interfaces. Furthermore, another very interesting aspect consists in being able to couple independent finite elements softwares, each dealing with its own subdomain and its own time integration scheme. These different space and time scales involve to develop numerical methods capable of handling these multiscale aspects. The proposed multiscale approach allows to view the global domain as an assembly of subdomains which may present different time discretizations and different time numerical schemes. Thus, the decomposition of the structure into subdomains enables one to use the most suitable time and space discretization for each subdomain. This, however, requires the existence of a mechanism capable of handling cases where the time and space discretizations of one subdomain are incompatible with those of its neighbors. Therefore, the difficulty in performing multiscale calculations consists in achieving communication among different models on different discretizations in order to recover the global response of the structure.

The differences among the available subdomains techniques reside in the treatment of the interface between the subdomains. One can distinguish two main approaches: with or without overlapping of the interfaces between subdomains. Among the techniques with overlapping, one may mention Schwarz-type methods [30] or Arlequin-type methods [6]. Among the techniques without overlapping, one can distinguish primal Schur-type approaches [12], where continuity of displacements is enforced at the interfaces, dual Schur-type approaches [27], where equilibrium of interfaces forces is

N. Mahjoubi · A. Gravouil · A. Combescure (✉)
Universite de Lyon, INSA-Lyon, LaMCoS CNRS UMR5259, Bât. Jean d'Alembert, 18-20 rue des Sciences, 69621 Villeurbanne, France
e-mail: alain.combescure@insa-lyon.fr

enforced with Lagrange multipliers, and mixed approaches [18], where one tries to achieve both conditions.

The FETI, a dual domain decomposition method (proposed initially by Farhat and Roux [13]), was developed for static problems, by dividing large domains into subdomains in order to optimize the resolution of linear systems on parallel-architecture computers. The FETI method can be viewed as an iterative solver where Lagrange multipliers are introduced in order to enforce a displacement continuity condition at the interfaces between subdomains. In a second step, the FETI method was extended to transient dynamic problems (see [14,15]).

In the context of the dual Schur-type approach, Gravouil and Combescure proposed a multi-time-scale method (GC method) in order to couple schemes of the Newmark family both for linear and nonlinear problems with a velocity continuity condition at the interfaces [20]. The stability property of this method was proven through an energy method (see [23,24]). Thus, it can be shown that the method ensures energy balance as long as the time discretization is the same for all subdomains. When each subdomain has its own time scale, the method is still stable. However for large ratio of time scales, numerical dissipation can occur at the interface. Furthermore, this method was extended to the cases of incompatible meshes, contact problems and modal methods (see [7,8,16,21,22]). In the works of Combescure et al. previously mentioned, the calculation may be performed with arbitrary and different pairs of parameters (γ, β) of the Newmark scheme [28] for each subdomain. Recently, Prakash and Hjelmstad [29] proposed a domain decomposition method (inspired by the GC method) which ensures that the work of the interface forces is zero for all schemes of the Newmark family with different time scales.

One can mention alternative simple methods for coupling explicit-implicit-type methods with different time scales (see [2,11]), either by applying nodal explicit-implicit partitioning [1] or by using explicit-implicit elements [24]. The method has been further extended and improved by Liu and coworkers [3–5]. One should nevertheless notice that one uses a single pair of parameters (γ, β) of the Newmark scheme for the whole structure. Furthermore, one can implement automatic refinement techniques (see [9,25]) which enable the automatic definition of a suitable time scale for a particular zone of the structure for a given numerical time scheme.

When different time scales occur for each subdomain, one inevitably comes to the question of the most appropriate numerical time integration scheme of each part. In practice, it can be very useful to couple two subdomains, the first one with an implicit integration scheme and the second one with an explicit integration scheme such as the central difference method when nonlinearities occur in a localized part of the structure.

The present article proposes a general formalism for a wide range of time numerical schemes which enables to couple subdomains with their own time integration scheme with large ratio of time scales. The decomposition method proposed is of the dual Schur type. In Sect. 1, we present the considered time schemes in order to establish this general formalism. This approach relies on the Lagrange multipliers formalism associated with continuity of velocities at the interfaces between subdomains. In Sect. 2, we present the coupling algorithm for three families of numerical time integration schemes. First, we study the case where all the subdomains have the same time scale. Then, we propose an extension of the proposed approach when different time scale occur. The multi-scale algorithm both for linear and nonlinear dynamic problems are detailed. A study of the accuracy and the convergence is also proposed for different time schemes and different time scales. Finally, Sect. 5, we illustrate the effectiveness and the robustness of the method through linear and nonlinear multi-time-scale examples.

2 Presentation of the integration schemes

In structural dynamics, the spatial finite element discretization of the structure leads to a system of second-order time differential equations. In order to solve this system, two approaches are usually considered. The first one consits in modal superposition [17], which uses a reduced basis of eigenmodes with a strong mechanical meaning, particularly in linear dynamics. This approach loses its interest in nonlinear dynamics because the eigenmodes must be reevaluated as the state of the system evolves with the possible nonlinear effects. The second approach is direct time integration, which is better suited in the case of high nonlinearities, but requires to control the accuracy and stability of the time scheme used. Direct time integration has been a very active research field for many years, and there are now many families of numerical time schemes available. It can be noticed that time numerical schemes can be distingushed in the following way: equilibrium equation is verified either in a "strong" sense, i.e. at time t_{n+1}, or in a "weak" sense, i.e. in an average way over the time interval $[t_n,\ t_{n+1}]$.

Among the most used numerical schemes are those of the Newmark family [28]. Approximate relations enable one to express the displacements $\mathbf{u}_{n+1}$, velocities $\dot{\mathbf{u}}_{n+1}$ and accelerations $\ddot{\mathbf{u}}_{n+1}$ at time t_{n+1} as functions of the kinematic quantities at time t_n. The advantage of this algorithm is its simplicity and its similarity with resolution techniques for quasi-static problems.

Another implicit time scheme dedicated to transient dynamics problems is the midpoint scheme proposed by Simo [31]. This scheme is unconditionally stable [31] when the material law possibly nonlinear, derives from a potential. The midpoint scheme seeks a solution of the equilibrium

equation at midpoint through the time interval $[t_n, t_{n+1}]$ and ensured the energy balance and kinetic moment at each time step.

More recently, a scheme written in the form of a state vector was proposed by Krenk [26]. This scheme introduces the independent variable $\mathbf{v}$ and enforces the relation $\mathbf{v} = \dot{\mathbf{u}}$ (where $\dot{\mathbf{u}}$ is the time derivative of the displacement $\mathbf{u}$). This last expression along with the equilibrium equation leads to an augmented system written in the form of a state vector $[\mathbf{u}^T,\ \mathbf{v}^T]$. In order to ensure energy balance, the augmented system is integrated over the time interval $[t_n,\ t_{n+1}]$. In addition, numerical damping can easily be introduced into the algorithm in the high frequency range while the dissipation in the low-frequency range is reduced [26].

In the present paper, we will use these three families of time schemes, which will be briefly presented in the following parts. The Lagrange multipliers will be used to represent either the boundary conditions of a dynamic problem or the continuity conditions which must be verified at the interfaces between the subdomains. The interface forces are linked to Lagrange multipliers and ensure the velocity continuity at the interfaces. Expressing continuity through the velocities at the interfaces is the key point in order to couple different time schemes with their own time scale (see [20,29]). From now on, we will refer to the Newmark, Simo and Krenk schemes by using the capital letters N, S and K respectively.

2.1 The Newmark scheme

The Newmark numerical time schemes consist of one time step approach and two parameters (γ and β). The state of the system at time $t_{n+1} = t_n + \Delta t$ is calculated as a function of the known state at time t_n. In order to do that, one uses Newmark's relations which, for example, give an approximation of the displacements $\mathbf{u}_{n+1}$ and accelerations $\ddot{\mathbf{u}}_{n+1}$ at time t_{n+1} as functions of the state of the system at time t_n and velocities $\dot{\mathbf{u}}_{n+1}$:

$$\mathbf{u}_{n+1} =^p \mathbf{u}_n + \frac{\beta}{\gamma}\Delta t\dot{\mathbf{u}}_{n+1} \tag{1}$$

$$\ddot{\mathbf{u}}_{n+1} =^p \ddot{\mathbf{u}}_n + \frac{1}{\gamma\Delta t}\dot{\mathbf{u}}_{n+1} \tag{2}$$

The displacement and acceleration predictors ${}^p\mathbf{u}_n$ and ${}^p\ddot{\mathbf{u}}_n$ are defined by:

$${}^p\mathbf{u}_n = \mathbf{u}_n + \Delta t\left(\frac{\gamma-\beta}{\gamma}\right)\dot{\mathbf{u}}_n + \left(\frac{\gamma-2\beta}{2\gamma}\right)\Delta t^2\ddot{\mathbf{u}}_n \tag{3}$$

$${}^p\ddot{\mathbf{u}}_n = \left(\frac{\gamma-1}{\gamma}\right)\ddot{\mathbf{u}}_n - \frac{1}{\gamma\Delta t}\dot{\mathbf{u}}_n \tag{4}$$

Then, Relations (1) and (2) are substituted into the equilibrium equation (5) at time t_{n+1}:

$$\mathbf{M}\ddot{\mathbf{u}}_{n+1} + \mathbf{K}\mathbf{u}_{n+1} = \mathbf{f}^{\text{ext}}_{n+1} + \mathbf{L}^T\boldsymbol{\lambda}_{n+1} \tag{5}$$

where $\mathbf{M}$, $\mathbf{K}$ and $\mathbf{f}^{\text{ext}}_{n+1}$ are the mass matrix, the stiffness matrix and the vector of external forces respectively. Matrices $\mathbf{M}$ and $\mathbf{K}$ are considered to be symmetrical; $\mathbf{M}$ is positive definite and $\mathbf{K}$ is positive semi-definite. The term $\mathbf{L}^T\boldsymbol{\lambda}_{n+1}$ in the equilibrium equation (5) corresponds to the interface forces. $\mathbf{L}$ is the interface operator which enables one to prescribe a condition over certain nodes of the structure (e.g. continuity at the interface nodes between subdomains) and $\boldsymbol{\lambda}_{n+1}$ is the vector of the corresponding Lagrange multipliers (mechanical damping is not considered here for simplicity reasons). After simplifying and adding the continuity equation written in terms of velocities, the system obtained can be written in the following form:

$$\begin{bmatrix}\tilde{\mathbf{M}}_N & -\mathbf{L}^T\\ -\mathbf{L} & \mathbf{0}\end{bmatrix}\begin{bmatrix}\dot{\mathbf{u}}_{n+1}\\ \boldsymbol{\lambda}_{n+1}\end{bmatrix} = \begin{bmatrix}\mathbf{f}^{\text{ext}}_{n+1} - \mathbf{K}^p\mathbf{u}_n - \mathbf{M}^p\ddot{\mathbf{u}}_n\\ -\dot{\mathbf{u}}^d_{n+1}\end{bmatrix} \tag{6}$$

The term $\dot{\mathbf{u}}^d_{n+1}$ in Eq. (6) represents the prescribed velocities at the interfaces. The dynamic operator $\tilde{\mathbf{M}}_N$ involved in the system (6) can be written as:

$$\tilde{\mathbf{M}}_N = \frac{1}{\gamma\Delta t}\mathbf{M} + \frac{\beta\Delta t}{\gamma}\mathbf{K} \tag{7}$$

2.2 The Simo scheme

In this presentation, the midpoint scheme is written for a linear problem for clarity sake. The equilibrium equation is verified at the mid point $t_{n+1/2}$ with:

$$\begin{aligned}&\frac{1}{2}\mathbf{M}\left(\ddot{\mathbf{u}}_{n+1} + \ddot{\mathbf{u}}_n\right) + \frac{1}{2}\mathbf{K}\left(\mathbf{u}_{n+1} + \mathbf{u}_n\right)\\ &\quad = \mathbf{f}^{\text{ext}}_{n+1/2} + \frac{1}{2}\mathbf{L}^T\left(\boldsymbol{\lambda}_{n+1} + \boldsymbol{\lambda}_n\right)\\ &\mathbf{f}^{\text{ext}}_{n+1/2} = \frac{1}{2}(\mathbf{f}^{\text{ext}}_{n+1} + \mathbf{f}^{\text{ext}}_n)\end{aligned} \tag{8}$$

In the equilibrium equation (8), the interfaces forces, inertia forces and internal forces are expressed at the midpoint. The equilibrium equation (8) is associated with the Newmark relations Eqs. (1) and (2) written with the parameters $\gamma = 1/2$ and $\beta = 1/4$ (average acceleration scheme):

$$\mathbf{u}_{n+1} = {}^p\mathbf{u}_n + \frac{\Delta t}{2}\dot{\mathbf{u}}_{n+1} \tag{9}$$

$$\ddot{\mathbf{u}}_{n+1} = {}^p\ddot{\mathbf{u}}_n + \frac{2}{\Delta t}\dot{\mathbf{u}}_{n+1} \tag{10}$$

In the same way as (6), one can write:

$$\begin{bmatrix}\tilde{\mathbf{M}}_S & -\mathbf{L}^T\\ -\mathbf{L} & \mathbf{0}\end{bmatrix}\begin{bmatrix}\dot{\mathbf{u}}_{n+1}\\ \boldsymbol{\lambda}_{n+1}\end{bmatrix} = \begin{bmatrix}2\mathbf{f}^{\text{ext}}_{n+1/2} + \mathbf{L}^T\boldsymbol{\lambda}_n - \mathbf{M}^p\ddot{\mathbf{u}}_n - \mathbf{K}^p\mathbf{u}_n - \mathbf{M}\ddot{\mathbf{u}}_n - \mathbf{K}\mathbf{u}_n\\ -\dot{\mathbf{u}}^d_{n+1}\end{bmatrix} \tag{11}$$

The dynamic operator $\tilde{\mathbf{M}}_S$ in the system of Eq. (11) can be written as:

$$\tilde{\mathbf{M}}_S = \frac{2}{\Delta t}\mathbf{M} + \frac{\Delta t}{2}\mathbf{K} \tag{12}$$

Let us observe that in this case the operator (12) is identical to the operator (7) with the parameters $\gamma = 1/2$ and $\beta = 1/4$ (average acceleration scheme).

2.3 The Krenk scheme

One recalls that the linear dynamic equilibrium equation discretized in space and continuous in time has the following form:

$$\mathbf{M}\ddot{\mathbf{u}}(t) + \mathbf{K}\mathbf{u}(t) = \mathbf{f}^{\text{ext}}(t) + \mathbf{L}^T\boldsymbol{\lambda}(t) \tag{13}$$

In order to transform the second-order equation (13) into a first-order equation, let us treat the velocity as an independent variable:

$$\mathbf{v} = \dot{\mathbf{u}} \tag{14}$$

The augmented system consists of Eq. (13) and the definition (14) multiplied by $\mathbf{M}$. This system is integrated over the time interval $[t_n, t_{n+1}]$. The resulting system is expressed as a state vector $[\mathbf{u}^T, \mathbf{v}^T]$ and can be written in the following form:

$$\begin{bmatrix} \mathbf{0} & \mathbf{M} & \mathbf{0} \\ \mathbf{M} & \mathbf{0} & \mathbf{0} \\ \mathbf{0} & \mathbf{L}/2 & \mathbf{0} \end{bmatrix} \begin{bmatrix} [\mathbf{u}_n] \\ [\mathbf{v}_n] \\ [\boldsymbol{\lambda}_n] \end{bmatrix} + \Delta t \begin{bmatrix} \mathbf{K} & \mathbf{0} & -\mathbf{L}^T \\ \mathbf{0} & -\mathbf{M} & \mathbf{0} \\ \mathbf{0} & \mathbf{L}/\Delta t & \mathbf{0} \end{bmatrix} \times \begin{bmatrix} \langle \mathbf{u}_n \rangle \\ \langle \mathbf{v}_n \rangle \\ \langle \boldsymbol{\lambda}_n \rangle \end{bmatrix} = \begin{bmatrix} \Delta t \langle \mathbf{f}_n^{\text{ext}} \rangle \\ 0 \\ 0 \end{bmatrix} \tag{15}$$

The jump and average operators in the system (15), respectively $[\bullet]$ and $\langle \bullet \rangle$, are defined by:

$$[\mathbf{x}_n] = \mathbf{x}_{n+1} - \mathbf{x}_n \quad \langle \mathbf{x}_n \rangle = (\mathbf{x}_{n+1} + \mathbf{x}_n)/2 \tag{16}$$

where $\mathbf{x}$ represents any discretized vector. In the case of the Krenk scheme, the interface forces are integrated over the time interval $[t_n, t_{n+1}]$ in the same way as the other quantities. The velocity continuity condition, third line of the system (15), is added to the augmented system defined above. This relation is not integrated over the time interval, but prescribed only for the velocity at time t_{n+1}. With the notations (16), we observe that:

$$\langle \mathbf{x}_n \rangle = \mathbf{x}_n + \frac{[\mathbf{x}_n]}{2} \tag{17}$$

Using Eq. (17), the second line of the system (15) can be expressed as:

$$\langle \mathbf{u}_n \rangle = \frac{\Delta t}{2} \langle \mathbf{v}_n \rangle + \mathbf{u}_n \tag{18}$$

Substituting the Eq. (18) into the first line of the system (15) and using the remark (17), one can write after simplification:

$$\left(\frac{2}{\Delta t}\mathbf{M} + \frac{\Delta t}{2}\mathbf{K}\right)\mathbf{v}_{n+1} - \mathbf{L}^T\boldsymbol{\lambda}_{n+1} = \left(2\mathbf{f}_{n+1/2}^{\text{ext}} + \mathbf{L}^T\boldsymbol{\lambda}_n + \mathbf{B}\mathbf{v}_n - 2\mathbf{K}\mathbf{u}_n\right)$$

$$\mathbf{f}_{n+1/2}^{\text{ext}} = \frac{1}{2}(\mathbf{f}_{n+1}^{\text{ext}} + \mathbf{f}_n^{\text{ext}}) \tag{19}$$

$$\mathbf{B} = \frac{2}{\Delta t}\mathbf{M} - \frac{\Delta t}{2}\mathbf{K}$$

From Eq. (15.b), one deduces the displacements $\mathbf{u}_{n+1}$:

$$\mathbf{u}_{n+1} = \mathbf{u}_n + [\mathbf{u}_n] \tag{20}$$

with:

$$[\mathbf{u}_n] = \frac{\Delta t}{2}[\mathbf{v}_n] + \Delta t\,\mathbf{v}_n \tag{21}$$

The Krenk time scheme can be written in a form equivalent to (11) as:

$$\begin{bmatrix} \tilde{\mathbf{M}}_K & -\mathbf{L}^T \\ -\mathbf{L} & \mathbf{0} \end{bmatrix} \begin{bmatrix} \mathbf{v}_{n+1} \\ \boldsymbol{\lambda}_{n+1} \end{bmatrix} = \begin{bmatrix} 2\mathbf{f}_{n+1/2}^{\text{ext}} + \mathbf{L}^T\boldsymbol{\lambda}_n - 2\mathbf{K}\mathbf{u}_n + \mathbf{B}\mathbf{v}_n \\ -\mathbf{v}_{n+1}^d \end{bmatrix} \tag{22}$$

In the system (22), the dynamic operator $\tilde{\mathbf{M}}_K$ can be written as:

$$\tilde{\mathbf{M}}_K = \frac{2}{\Delta t}\mathbf{M} + \frac{\Delta t}{2}\mathbf{K} \tag{23}$$

One can observe that the expression of the matrix $\tilde{\mathbf{M}}_K$ given by (23) is the same as the one obtained with the midpoint scheme (Eq. 12).

2.4 Energy balance

In order to measure the numerical dissipation introduced by a time numerical scheme, it is necessary to define a discretized energy balance. In this respect, one introduces the discretized kinetic energy, the discretized internal energy and the work of the external forces. In the linear dynamic case, these quantities are defined respectively as:

$$\begin{aligned} \mathcal{T}(\dot{\mathbf{u}}) &= \frac{1}{2}\dot{\mathbf{u}}^T\mathbf{M}\dot{\mathbf{u}} \\ \mathcal{V}(\mathbf{u}) &= \frac{1}{2}\mathbf{u}^T\mathbf{K}\mathbf{u} \\ \mathcal{W}(\dot{\mathbf{u}}) &= \dot{\mathbf{u}}^T\mathbf{f}^{\text{ext}} \end{aligned} \tag{24}$$

In order to define the discretized energy balance using the previous notations (16), one can consider the variation of the kinetic and internal energies between t_n and t_{n+1}:

$$[\mathcal{T}(\dot{\mathbf{u}}_n)] = [\dot{\mathbf{u}}_n]^T\,\mathbf{M}\,\langle \dot{\mathbf{u}}_n \rangle \tag{25}$$

$$[\mathcal{V}(\mathbf{u}_n)] = [\mathbf{u}_n]^T\,\mathbf{K}\,\langle \mathbf{u}_n \rangle \tag{26}$$

Then, one can define the variation of the total energy as:

$$[\mathcal{E}(\mathbf{u}_n, \dot{\mathbf{u}}_n)] = [\mathcal{T}(\dot{\mathbf{u}}_n)] + [\mathcal{V}(\mathbf{u}_n)] \tag{27}$$

The work of the external forces is obtained by calculating the integral:

$$\Delta\mathcal{W}_{\text{ext}(n\to n+1)} = \int_n^{n+1} \dot{\mathbf{u}}^T \mathbf{f}^{\text{ext}}\, \mathrm{dt} \tag{28}$$

The calculation of this integral depends on the discretization of the kinematic quantities associated with the schemes presented before. The associated expressions can be written in the following form:

$$\Delta\mathcal{W}^N_{\text{ext}(n\to n+1)} = [\mathbf{u}_n]^T \langle \mathbf{f}^{\text{ext}}_n \rangle + \left(\gamma - \frac{1}{2}\right) [\mathbf{u}_n]^T \left[\mathbf{f}^{\text{ext}}_n\right] \tag{29}$$

$$\Delta\mathcal{W}^S_{\text{ext}(n\to n+1)} = [\mathbf{u}_n]^T \langle \mathbf{f}^{\text{ext}}_n \rangle \tag{30}$$

$$\Delta\mathcal{W}^K_{\text{ext}(n\to n+1)} = [\mathbf{u}_n]^T \langle \mathbf{f}^{\text{ext}}_n \rangle \tag{31}$$

where N, S and K correspond respectively to Newmark, Simo and Krenk numerical time schemes. In case of non dissipative physical phenomena, it is interesting to calculate the difference between the variation of the mechanical energy and the work of the external forces between times t_n and t_{n+1}. This enables one to quantify the numerical dissipation introduced either by the scheme or by the work of the interface forces, whose calculation is the same as for the external forces.

We will calculate these quantities for the presented numerical examples in order to assess the accuracy and stability of the coupling method for different time scales and different time schemes.

3 General method for subdomain coupling

One considers here a dual Schur domain decomposition method for coupling different time numerical schemes with their own time discretization. For such a formulation, the question of the kinematic quantity whose continuity must be prescribed at the interface arises. In continuum mechanics, prescribing continuity displacements at the interface leads to continuous velocities and accelerations. This is no longer true for the equivalent discretized quantities in time. Prescribing that one of the three kinematic quantities (displacements, velocities or accelerations) is continuous does not automatically mean that the other two are continuous. We propose here to ensure the continuity of the discretized velocity in a Schur dual formulation (see [19,20]). It will be shown that this is a judicious choice for the purpose of assembling subdomains with different time integration schemes.

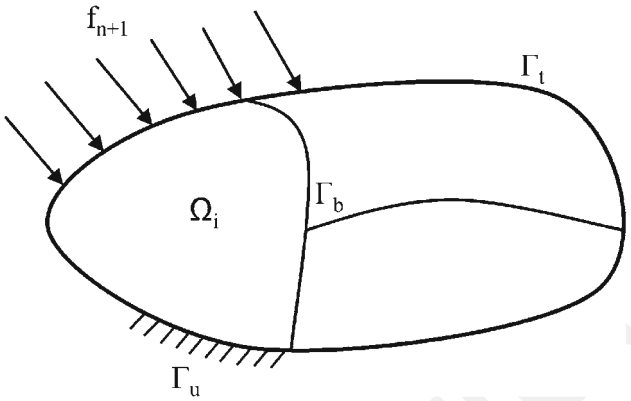

Fig. 1 A domain Ω divided into three subdomains with the interface Γ_b among the subdomains

3.1 Same time scale for all subdomains

Let us consider a domain Ω divided into three subdomains with their own time integration scheme according to the time schemes presented in the previous sections. In the following matrix equations, the boundary conditions of the problem do not appear explicitly. The interface forces between the subdomains are linked to the discretized Lagrange multipliers $\boldsymbol{\lambda}$. Figure 1 displays a typical subdomain decomposition where $\mathbf{f}_{n+1}$ is the external load, Γ_u the boundary of the domain Ω on which the displacements are prescribed, Γ_t the boundary where the traction forces are prescribed. Γ_b is the interface between the subdomains and Ω_i with $i \in \{N,\ S,\ K\}$.

$$\begin{bmatrix} \tilde{\mathbf{M}}_N & \mathbf{0} & \mathbf{0} & -\mathbf{L}_N^T \\ \mathbf{0} & \tilde{\mathbf{M}}_S & \mathbf{0} & -\mathbf{L}_S^T \\ \mathbf{0} & \mathbf{0} & \tilde{\mathbf{M}}_K & -\mathbf{L}_K^T \\ -\mathbf{L}_N & -\mathbf{L}_S & -\mathbf{L}_K & \mathbf{0} \end{bmatrix} \begin{bmatrix} \dot{\mathbf{u}}^N_{n+1} \\ \dot{\mathbf{u}}^S_{n+1} \\ \dot{\mathbf{u}}^K_{n+1} \\ \boldsymbol{\lambda}_{n+1} \end{bmatrix} = \begin{bmatrix} \mathbf{F}^N_{n+1} \\ \mathbf{F}^S_{n+1} \\ \mathbf{F}^K_{n+1} \\ \mathbf{0} \end{bmatrix} \tag{32}$$

$$\begin{cases} \mathbf{F}^N_{n+1} = \mathbf{f}^{N/\text{ext}}_{n+1} - \mathbf{M}_N{}^p \ddot{\mathbf{u}}^N_n - \mathbf{K}_N{}^p \mathbf{u}^N_n \\ \mathbf{F}^S_{n+1} = 2\mathbf{f}^{S/\text{ext}}_{n+1/2} + \mathbf{L}_S^T \boldsymbol{\lambda}_n - \mathbf{M}_S^p \ddot{\mathbf{u}}^S_n \\ \qquad\qquad -\mathbf{K}_S^p \mathbf{u}^S_n - \mathbf{M}_S \ddot{\mathbf{u}}^S_n - \mathbf{K}_S \mathbf{u}^S_n \\ \mathbf{F}^K_{n+1} = 2\mathbf{f}^{K/\text{ext}}_{n+1/2} + \mathbf{L}_K^T \boldsymbol{\lambda}_n + \mathbf{B}\mathbf{v}_n - 2\mathbf{K}_K \mathbf{u}_n \end{cases} \tag{33}$$

The subscripts of the matrices and the superscripts of the vector quantities indicate the numerical time scheme used. It was shown in [10] that if Newmark time schemes are being used with prescribed continuity of discretized velocities at the interface between the subdomains guarantees the stability of the coupling method. In this work, we intend to use, in addition to schemes of the Newmark family, the schemes which were presented in the previous Sects. 2.1–2.3 in a more general formalism. Similarly, we prescribe the continuity of velocities at the interfaces between all integration schemes.

The last line of the system (32) enables to prescribe the continuity of velocities at the interfaces between the subdomains. The Lagrange multipliers $\boldsymbol{\lambda}_{n+1}$ correspond to the interface forces between each subdomain. The terms on the right-hand side of the system (32), detailed in expressions (33), depend on external loads and on quantities which are known at time t_n.

The strategy used in order to solve the system (32) consists in decomposing the problem into an unconstrained problem (free) and a problem with constraints (link). Indeed, each kinematic quantity can be viewed as the sum of two terms:

$$\dot{\mathbf{u}}^i_{n+1} = \dot{\mathbf{u}}^i_{n+1/\text{free}} + \dot{\mathbf{u}}^i_{n+1/\text{link}} \qquad \forall i \in \{N, S, K\} \tag{34}$$

where the free term $\dot{\mathbf{u}}^i_{n+1/\text{free}}$ is the solution of the free problem subject to the external loading and the term of the problem with constraints $\dot{\mathbf{u}}^i_{n+1/\text{link}}$ is obtained by applying the interface forces. This decomposition into an unconstrained problem and a problem with constraints can be presented in the following form:

1. The unconstrained problem can be written as:

$$\begin{bmatrix} \tilde{\mathbf{M}}_N & \mathbf{0} & \mathbf{0} & \mathbf{0} \\ \mathbf{0} & \tilde{\mathbf{M}}_S & \mathbf{0} & \mathbf{0} \\ \mathbf{0} & \mathbf{0} & \tilde{\mathbf{M}}_K & \mathbf{0} \\ \mathbf{0} & \mathbf{0} & \mathbf{0} & \mathbf{0} \end{bmatrix} \begin{bmatrix} \dot{\mathbf{u}}^N_{n+1/\text{free}} \\ \dot{\mathbf{u}}^S_{n+1/\text{free}} \\ \dot{\mathbf{u}}^K_{n+1/\text{free}} \\ \boldsymbol{\lambda}_{n+1} \end{bmatrix} = \begin{bmatrix} \mathbf{F}^N_{n+1} \\ \mathbf{F}^S_{n+1} \\ \mathbf{F}^K_{n+1} \\ \mathbf{0} \end{bmatrix} \tag{35}$$

   The structure of the system (35) enables the resolution of the unconstrained problem independently over each subdomain. Thus, given the velocities of the unconstrained problems on the boundary of each subdomain, the other kinematic quantities can be deduced using relations which are specific to the time integration scheme (see Sects. 2.1–2.3).
2. The constrained problem can be written as:

$$\begin{bmatrix} \tilde{\mathbf{M}}_N & \mathbf{0} & \mathbf{0} & -\mathbf{L}^T_N \\ \mathbf{0} & \tilde{\mathbf{M}}_S & \mathbf{0} & -\mathbf{L}^T_S \\ \mathbf{0} & \mathbf{0} & \tilde{\mathbf{M}}_K & -\mathbf{L}^T_K \\ -\mathbf{L}_N & -\mathbf{L}_S & -\mathbf{L}_K & \mathbf{0} \end{bmatrix} \begin{bmatrix} \dot{\mathbf{u}}^N_{n+1/\text{link}} \\ \dot{\mathbf{u}}^S_{n+1/\text{link}} \\ \dot{\mathbf{u}}^K_{n+1/\text{link}} \\ \boldsymbol{\lambda}_{n+1} \end{bmatrix} = \begin{bmatrix} \mathbf{0} \\ \mathbf{0} \\ \mathbf{0} \\ \sum_i \mathbf{L}_i \dot{\mathbf{u}}^i_{n+1/\text{free}} \end{bmatrix} \tag{36}$$

   Thus, the system (36) enables the calculation of the correction terms to be added to the quantities of the free system previously obtained (see Eq. 35). In order to do that, a first step consists in calculating the interface forces through the Lagrange multipliers $\boldsymbol{\lambda}_{n+1}$, which requires a condensation step over the interface Γ_b between the subdomains. In this respect, the condensed problem at the interface can be expressed as:

$$\mathbf{H}\,\boldsymbol{\lambda}_{n+1} = \mathbf{b}_{n+1} \tag{37}$$

where the condensation operator $\mathbf{H}$ (i.e. the Steklov-Poincaré operator) and the right-hand side $\mathbf{b}_{n+1}$ can be given by:

$$\mathbf{H} = \sum_i \mathbf{L}_i \left[a_i \mathbf{M}_i + b_i \mathbf{K}_i\right]^{-1} \mathbf{L}^T_i \tag{38}$$

$$\mathbf{b}_{n+1} = -\sum_i \mathbf{L}_i \dot{\mathbf{u}}^i_{n+1/\text{free}} \tag{39}$$

where a_i and b_i are two coefficients which depend on the considered time scheme as indicated in Table 1.

Table 1 Coefficients a_i and b_i

Scheme	a_i	b_i
Newmark	$\frac{1}{\gamma \Delta t}$	$\frac{\beta \Delta t}{\gamma}$
Simo	$\frac{2}{\Delta t}$	$\frac{\Delta t}{2}$
Krenk	$\frac{2}{\Delta t}$	$\frac{\Delta t}{2}$

Let us observe that the condensation operator $\mathbf{H}$ is obtained as the sum of the condensation operator of each subdomain. One can also note that for the average acceleration scheme ($\gamma = 1/2$ and $\beta = 1/4$), the midpoint scheme and Krenk's scheme the condensation operators have identical coefficients a_i and b_i and can be expressed in the form:

$$\mathbf{H} = \mathbf{L}\left[\frac{2}{\Delta t}\mathbf{M} + \frac{\Delta t}{2}\mathbf{K}\right]^{-1} \mathbf{L}^T \tag{40}$$

The approach presented above can be extended without major difficulty to any number of subdomains.

Remark 1 One must observe that if the method is applied to couple only incompatible explicit time schemes the coupled problem solution implies formal inversion of matrix $\mathbf{H}$. Hence the price to pay for this type of coupling is to solve a linear system (associated to the matrix $\mathbf{H}$). Nevertheless this matrix is proportional to the time step it is hence constant in time in case of linear explicit computation: this induces the idea that a direct method can be chosen and hence the matrix is "inverted" only once.

Remark 2 Let us insist that the kinematic constraints are applied on the velocities: this implies that the continuity of the displacement and acceleration are not impose in a strong sense. And the kinematics of these quantities may be not exactly the same at the interface.

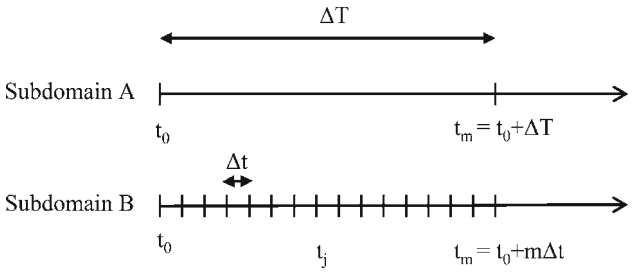

Fig. 2 Time-hierarchical meshes

Table 2 Dynamic operators

Time scheme	Dynamic operator
Newmark	$\frac{1}{\gamma \Delta t}\mathbf{M} + \frac{\beta \Delta t}{\gamma}\mathbf{K}$
Simo	$\frac{2}{\Delta t}\mathbf{M} + \frac{\Delta t}{2}\mathbf{K}$
Krenk	$\frac{2}{\Delta t}\mathbf{M} + \frac{\Delta t}{2}\mathbf{K}$

3.2 Independent time scales for each subdomain

The main interest of the proposed coupling method is on the one hand to couple different time numerical schemes with their own properties of stability and accuracy and on the other hand to couple different time discretization subdomain by subdomain. It can be very interesting for instance to couple explicit subdomains with their own time scale depending on the possible localized nonlinearities or high frequency properties of each subdomain. In this case, the equilibrium equation of a subdomain is verified at instants which can differ from those of its neighbors. Thus, the difficulty resides in establishing proper communication among subdomains with different time scales. A strategy which allows to achieve such a communication was developed by Gravouil [20] and was also used in this work. In order to introduce this technique, let us consider two subdomains A and B with their respective time steps Δt and ΔT such that $\Delta T = m\Delta t$ (Fig. 2), m being an integer greater than one. When $m = 1$, the method is identical to that presented in Sect. 3.1. From now on, we will refer to a macro time scale (ΔT) for subdomain A and a micro time scale (Δt) for subdomain B.

Within the framework of the subdomain coupling technique proposed in Sect. 3.1, the equilibrium equations of subdomains A and B can be expressed in the general form:

$$\tilde{\mathbf{M}}_A \dot{\mathbf{u}}_m^A = \mathbf{F}_m^A \tag{41}$$

$$\tilde{\mathbf{M}}_B \dot{\mathbf{u}}_j^B = \mathbf{F}_j^B \quad \forall j \in \{1 \dots m\} \tag{42}$$

From (32), we can use for subdomains A and B any two of the three schemes studied in the present work. Depending on the scheme being considered, the right-hand sides of Eqs. (41) and (42) are given in expressions (33). The operators $\tilde{\mathbf{M}}_i$ are summarized in Table 2.

The incompatibility of the discretized instants between the macro and micro time scales requires the definition of an interpolation operator from the macroscale to the microscale. This interpolation at time t_j can be linear, as proposed in [19]. In this case, the resolution of the interface problem is carried out on the micro time scale. This interpolation operator can be defined by:

$$\dot{\mathbf{u}}_j = \left(1 - \frac{j}{m}\right)\dot{\mathbf{u}}_0 + \frac{j}{m}\dot{\mathbf{u}}_m \tag{43}$$

Thus, for a time step ΔT (on the macro time scale), m time steps Δt (on the micro time scale) have to be calculated. The method is similar to that proposed in [19], which can be summarized in the following algorithm where a single time step ΔT of the macro time scale is considered:

a. Resolution of the unconstrained problem on the subdomain A at time t_m

$$\tilde{\mathbf{M}}_A \dot{\mathbf{u}}_{m/\text{free}}^A = \mathbf{F}_m^A \tag{44}$$

The other free kinematic quantities of the subdomain A (displacement $\mathbf{u}_{m/\text{free}}^A$ and acceleration $\ddot{\mathbf{u}}_{m/\text{free}}^A$) can be obtained from the expressions given Sects. 2.1–2.3.

b. Loop over the m time steps of the subdomain B at time $t_j \quad j \in \forall\{1, \dots, m\}$.

c. Resolution of the unconstrained problem of the subdomain B at time t_j

$$\tilde{\mathbf{M}}_B \dot{\mathbf{u}}_{j/\text{free}}^B = \mathbf{F}_j^B \tag{45}$$

d. Interpolation of the free velocities of the subdomain A from the macro-scale to the micre-scale

$$\dot{\mathbf{u}}_{j/\text{free}}^A = \left(1 - \frac{j}{m}\right)\dot{\mathbf{u}}_{0/\text{free}}^A + \frac{j}{m}\dot{\mathbf{u}}_{m/\text{free}}^A \tag{46}$$

e. Calculation of the Lagrange multipliers $\boldsymbol{\lambda}_j$ on the problem condensed at the interface

$$\mathbf{H}\boldsymbol{\lambda}_j = -\sum_{i \in \{A,B\}} \mathbf{L}_i \dot{\mathbf{u}}_{j/\text{free}}^i \tag{47}$$

f. Resolution of the problem with constraints on the subdomain B at time t_j

$$\tilde{\mathbf{M}}_B \dot{\mathbf{u}}_{j/\text{link}}^B = \mathbf{L}_B^T \boldsymbol{\lambda}_j \tag{48}$$

After calculation of the kinematic quantities of the problem with constraints ($\mathbf{u}_{m/\text{link}}^B$ and $\ddot{\mathbf{u}}_{m/\text{link}}^B$), one can deduce

the kinematic quantities of the global problem on subdomain B.

$$\begin{cases} \mathbf{u}_j^B = \mathbf{u}_{j/\text{free}}^B + \mathbf{u}_{j/\text{link}}^B \\ \dot{\mathbf{u}}_j^B = \dot{\mathbf{u}}_{j/\text{free}}^B + \dot{\mathbf{u}}_{j/\text{link}}^B \\ \ddot{\mathbf{u}}_j^B = \ddot{\mathbf{u}}_{j/\text{free}}^B + \ddot{\mathbf{u}}_{j/\text{link}}^B \end{cases} \tag{49}$$

g. If $j = m$, end of loop
h. Resolution of the problem with constraints on subdomain A

$$\tilde{\mathbf{M}}_A \dot{\mathbf{u}}_{m/\text{link}}^A = \mathbf{L}_A^T \boldsymbol{\lambda}_m \tag{50}$$

After calculation of the other kinematic quantities of the problem with constraints ($\mathbf{u}_{m/\text{link}}^A$ and $\ddot{\mathbf{u}}_{m/\text{link}}^A$), one can deduce the kinematic quantities of the global problem on the subdomain A.

$$\begin{cases} \mathbf{u}_m^A = \mathbf{u}_{m/\text{free}}^A + \mathbf{u}_{m/\text{link}}^A \\ \dot{\mathbf{u}}_m^A = \dot{\mathbf{u}}_{m/\text{free}}^A + \dot{\mathbf{u}}_{m/\text{link}}^A \\ \ddot{\mathbf{u}}_m^A = \ddot{\mathbf{u}}_{m/\text{free}}^A + \ddot{\mathbf{u}}_{m/\text{link}}^A \end{cases} \tag{51}$$

This method can be generalized to s subdomains with hierarchical time scales with respect to the coarsest scale, such that:

$$\begin{cases} \Delta t_1 = \Delta t \\ \Delta t_2 = m_2 \Delta t \\ \vdots \\ \Delta t_s = m_s \Delta t \end{cases} \tag{52}$$

where $\{m_2, \ldots, m_s\} \in N^{*s-1}$. In this case, the algorithm is slightly more complex to implement than the presented above with two subdomains. However the implementation is roughly the same. Contrary to the static case (FETI method), one can observe that in the approach proposed here the interface problem is not solved iteratively with preconditioners. Indeed, for linear transient dynamics problems, since the condensation operator $\mathbf{H}$ remains constant along time, a direct resolution technique can be considered for the problem condensed at the interface. Thus, it is possible to triangularize the operator $\mathbf{H}$ only once in the initialization step. Then, standard direct solvers can be used to optimize the CPU time on the interface resolution.

The GC method is known to dissipate energy in case of Newmark time schemes with different time steps. It is then obvious that the proposed heterogeneous scheme coupling will dissipate energy as in case of Newmark schemes alone.

3.3 Nonlinear multi-time-scale analysis

The aim of this paragraph is to extend the proposed coupling method to the nonlinear case. Here, only a nonlinear behavior in the bulk will be considered (plasticity for instance). In [19], Gravouil proposed a domain decomposition method of the dual Schur type in order to couple arbitrary numerical schemes of the Newmark family in nonlinear analysis. Following the general formalism (see Eq. 32) given for domain decomposition with the Newmark, Simo and Krenk schemes, the extension of the GC method can be achieved in the same way. Let us assume that a nonlinear behavior (e.g. elastic-plastic with kinematic strain hardening) is associated with some localized zones of the structure. The corresponding subdomains can be associated with explicit numerical time schemes over a fine time scale required by the critical time step. These "explicit" subdomains can be coupled with the subdomains of the rest of the structure for which linear behavior with a coarse time scale is assumed. In fact, this is a generalization of the linear algorithm given in Sect. 3.2. In other words, let us consider two subdomains with two time scales (see Fig. 2). On the micro time scale, let us assume a nonlinear (elasto-plastic) behavior with a time step Δt and the explicit central difference scheme ($\gamma = 1/2$ and $\beta = 0$). On the subdomain with the macro time scale ΔT ($\Delta T = m\Delta t$, with $m \in N^*$) one assumes a linear constitutive law. On the "implicit" subdomain (I), one of the implicit schemes presented before is used (Newmark, Simo, Krenk). On the "explicit" subdomain (E), the equilibrium equation with the Newmark central difference numerical scheme can be expressed at time t_j as:

$$\begin{aligned} &\mathbf{M}_E \ddot{\mathbf{u}}_j^E + \mathbf{F}_{int\,j}^E \left({}^p\mathbf{u}_{j-1}^E \right) \\ &= \mathbf{f}_{\text{ext}\,j}^E + \mathbf{L}^T \boldsymbol{\lambda}_{n+1} \quad \text{with } \mathbf{M}_E \text{ the diagonal mass matrix} \end{aligned} \tag{53}$$

$$\begin{cases} \mathbf{u}_j^E = {}^p\mathbf{u}_{j-1}^E \\ \ddot{\mathbf{u}}_j^E = {}^p\ddot{\mathbf{u}}_{j-1}^E + \frac{1}{\gamma \Delta t} \dot{\mathbf{u}}_j^E \end{cases} \tag{54}$$

This method can be summarized for a given time step ΔT of the coarse time scale as follows:

a. Resolution of the unconstrained problem on the subdomain I at time t_m

$$\tilde{\mathbf{M}}_I \dot{\mathbf{u}}_{m/\text{free}}^I = \mathbf{F}_m^I \tag{55}$$

The other free kinematic quantities of the subdomain I (displacement $\mathbf{u}_{m/\text{free}}^I$ and acceleration $\ddot{\mathbf{u}}_{m/\text{free}}^I$) can be obtained from the expressions given in Sects. 2.1–2.3.
b. Loop over the m time steps of the subdomain E at time $t_j \quad j \in \forall\{1, \ldots, m\}$.
c. Resolution of the unconstrained problem on the subdomain E at time t_j

$$\mathbf{M}_E \ddot{\mathbf{u}}_{j/\text{free}}^E = \mathbf{f}_{\text{ext}\,j}^E - \mathbf{F}_{\text{int}\,j}^E \left({}^p\mathbf{u}_{j-1}^E \right) \tag{56}$$

d. Interpolation of the free velocities of the subdomain I:

$$\dot{\mathbf{u}}^I_{j/\text{free}} = \left(1 - \frac{j}{m}\right)\dot{\mathbf{u}}^I_{0/\text{free}} + \frac{j}{m}\dot{\mathbf{u}}^I_{m/\text{free}} \tag{57}$$

e. Calculation of the Lagrange multipliers $\boldsymbol{\lambda}_j$ of the problem condensed at the interface

$$\mathbf{H}\boldsymbol{\lambda}_j = -\sum_{i\in\{I,E\}} \mathbf{L}_i \dot{\mathbf{u}}^i_{j/\text{free}} \tag{58}$$

f. Resolution of the problem with constraints on the subdomain E at time t_j

$$\mathbf{M}_E \dot{\mathbf{u}}^E_{j/\text{link}} = \mathbf{L}^T_E \boldsymbol{\lambda}_j \tag{59}$$

After calculation of the kinematic quantities $\mathbf{u}^E_{j/\text{link}l}$ and $\ddot{\mathbf{u}}^E_{j/\text{link}}$, one can deduce the kinematic quantities of the global problem on the subdomain E.

$$\begin{cases} \mathbf{u}^E_j = \mathbf{u}^E_{j/\text{free}} + \mathbf{u}^E_{j/\text{link}} \\ \dot{\mathbf{u}}^E_j = \dot{\mathbf{u}}^E_{j/\text{free}} + \dot{\mathbf{u}}^E_{j/\text{link}} \\ \ddot{\mathbf{u}}^E_j = \ddot{\mathbf{u}}^E_{j/\text{free}} + \ddot{\mathbf{u}}^E_{j/\text{link}} \end{cases} \tag{60}$$

g. If $j = m$, end of loop

h. Resolution of the problem with constraints on the subdomain I

$$\tilde{\mathbf{M}}_I \dot{\mathbf{u}}^I_{m/\text{link}} = \mathbf{L}^T_I \boldsymbol{\lambda}_m \tag{61}$$

After calculation of the kinematic quantities $\mathbf{u}^I_{m/\text{link}}$ and $\ddot{\mathbf{u}}^I_{m/\text{link}}$, one can deduce the kinematic quantities of the global problem on the subdomain I.

$$\begin{cases} \mathbf{u}^I_m = \mathbf{u}^I_{m/\text{free}} + \mathbf{u}^I_{m/\text{link}} \\ \dot{\mathbf{u}}^I_m = \dot{\mathbf{u}}^I_{m/\text{free}} + \dot{\mathbf{u}}^I_{m/\text{link}} \\ \ddot{\mathbf{u}}^I_m = \ddot{\mathbf{u}}^I_{m/\text{free}} + \ddot{\mathbf{u}}^I_{m/\text{link}} \end{cases} \tag{62}$$

The condensation operator $\mathbf{H}$ is given by:

$$\mathbf{H} = \mathbf{L}_I \tilde{\mathbf{M}}_I^{-1} \mathbf{L}^T_I + \mathbf{L}_E \mathbf{M}_E^{-1} \mathbf{L}^T_E \tag{63}$$

It can be noticed that the algorithm is very similar to the linear case. Indead, only the lumped mass matrix $\mathbf{M}_E$ is required in the $\mathbf{H}$ interface operator for the explicit nonlinear subdomain E.

Remark for explicit subdomains the final displacement state is known at the beginning of the time step. All nonlinear effects can be computed before the link force application. These constraint loads will only change the computation of velocities and accelerations at the end of the time step and will hence have an effect on next time step.

3.4 Control of the interface numerical dissipation

In the previous sections, we developed a domain decomposition method of the dual Schur type in order to couple, under the same general formalism, arbitrary numerical schemes of the Newmark, Krenk and Simo families, with possible nonlinearities and different time scales. In this context, we showed that the incompatible discrete instants of the macro and micro time scales require the definition of a kinematic interpolation operator between the two time scales (Eq. 43). One can also note that the "free"/"link" uncoupling (Eq. 34) and the interpolation of the Lagrange multipliers require a resolution on the fine time scale at the interface. Recent works by Prakash and Hjelmstad [29] led to a method (the PH method) which makes the interface numerical dissipation in multi-time-scale calculations be zero with different time schemes of the Newmark family in linear elasticity, thanks to a slight modification of the "free"/"link" uncoupling. As the approach proposed by Gravouil and Combescure (the GC method), continuity of the velocities is prescribed at the interfaces. A linear interpolation similar but slightly different to Eq. 46 is implemented. Table 3 illustrates the details of the "free"/"link" uncoupling for the two approaches, GC and PH method through the interpolation relations used. In both cases, we obtain the interpolation relation among the global kinematic quantities defined by Eq. (43). For the PH method, the system to be solved for the coupling of two time-incompatible subdomains can be expressed in the form:

$$\begin{bmatrix} \mathbb{M} & \mathbb{C} \\ \mathbb{B} & \mathbf{0} \end{bmatrix} \begin{bmatrix} \mathbb{U} \\ \lambda_m \end{bmatrix} = \begin{bmatrix} \mathbb{P} \\ \mathbf{0} \end{bmatrix} \tag{64}$$

Here $\mathbb{U}$ represents the generalized vector: $\mathbb{U}^T = [\mathbf{u}^T,\ \dot{\mathbf{u}}^T,\ \ddot{\mathbf{u}}^T]$ In the case of Newmark type schemes, the definition of the vectors and matrices $\mathbb{M}$, $\mathbb{C}$, $\mathbb{B}$ and $\mathbb{P}$ are given in [29].

In order to obtain the system of Eq. (64) of the PH method, the Lagrange multipliers $\boldsymbol{\lambda}_j$ over the fine time scale are calculated using the Lagrange multipliers λ_m of the coarse time scale and the unbalanced interface reactions. The unbalanced interface reactions can be viewed as the amount by which the

Table 3 Compared coupling strategies 'free'/'link'

	GC	PH
Free	$\dot{\mathbf{u}}_{j/\text{free}} = \left(1 - \frac{j}{m}\right)\dot{\mathbf{u}}_{0/\text{free}} + \frac{j}{m}\dot{\mathbf{u}}_{m/\text{free}}$	$\dot{\mathbf{u}}_{j/\text{free}} = \left(1 - \frac{j}{m}\right)\dot{\mathbf{u}}_0 + \frac{j}{m}\dot{\mathbf{u}}_{m/\text{free}}$
Link	$\dot{\mathbf{u}}_{j/\text{link}} = \left(1 - \frac{j}{m}\right)\dot{\mathbf{u}}_{0/\text{link}} + \frac{j}{m}\dot{\mathbf{u}}_{m/\text{link}}$	$\dot{\mathbf{u}}_{j/\text{link}} = \frac{j}{m}\dot{\mathbf{u}}_{m/\text{link}}$

Fig. 3 A split SDOF problem

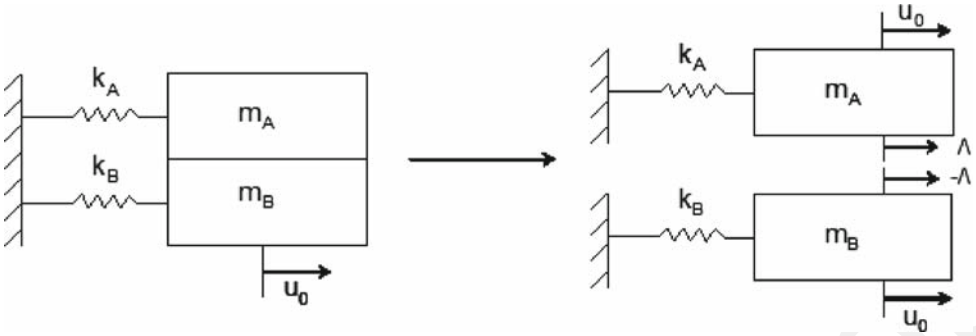

subdomain on the coarse time scale is out of force equilibrium at t_j under external forces only. These reactions can also be interpreted as the unbalance of a subdomain when this subdomain is subjected only to external forces.

In order to solve the system (64), one sets (65):

$$\begin{aligned} &\mathbb{U} = \mathbb{U}_{\text{free}} + \mathbb{U}_{\text{link}} \\ &\mathbb{U}_{\text{free}} = \mathbb{M}^{-1}\mathbb{P} \\ &\mathbb{U}_{\text{link}} = -\mathbb{Y}\lambda_m \quad and \quad \mathbb{Y} = \mathbb{M}^{-1}\mathbb{C} \end{aligned} \tag{65}$$

One deduces the condensed problem on the interface with:

$$[\mathbb{B}\mathbb{Y}]\,\lambda_m = \mathbb{B}\mathbb{U}_{\text{free}} \tag{66}$$

The main consequence can be summarized in two points: first, contrary to the GC method, the condensed problem at the interface is written on the coarse time scale. Second, by an energy method as in [29], one can also show that the PH method doesn't dissipate numerical energy at the interface when numerical time schemes of the Newmark family and/or different time scales are coupled in linear problems.

3.5 Consistency of the presented multi-time scales domain decomposition method

In this section, we study the consistency of the coupling method presented in the previous section. A numerical discretization in time of the transient dynamics problem consists in the equilibrium equation and the following relations for a one step algorithm:

$$\begin{aligned} &\dot{\mathbf{u}}_{n+1} = f(\dot{\mathbf{u}}_n, \ddot{\mathbf{u}}_n, \ddot{\mathbf{u}}_{n+1}) \\ &\mathbf{u}_{n+1} = f(\mathbf{u}_n,\ \dot{\mathbf{u}}_n,\ \dot{\mathbf{u}}_{n+1},\ \ddot{\mathbf{u}}_n,\ \ddot{\mathbf{u}}_{n+1}) \end{aligned} \tag{67}$$

A time numerical scheme is consistent if:

$$\lim_{h\to 0} \frac{\mathbf{U}_{n+1} - \mathbf{U}_n}{h} = \dot{\mathbf{U}}_n \tag{68}$$

where $\mathbf{U}_n^T = [\mathbf{u}_n, \dot{\mathbf{u}}_n]$ is the considered state vector.

The consistency can be studied by using a single degree of freedom (SDOF) problem. This system is composed of a mass (m) and a spring (k). For the unforced undamped SDOF system, the equation of motion becomes,

$$\begin{aligned} &\ddot{\mathbf{u}} + \omega^2\mathbf{u} = 0 \\ &\omega = \sqrt{k/m} \end{aligned} \tag{69}$$

with the initial conditions,

$$\begin{cases} \mathbf{u}(t=0) = \mathbf{u}_0 \\ \dot{\mathbf{u}}(t=0) = \dot{\mathbf{u}}_0 \end{cases} \tag{70}$$

In order to study the consistency of the presented domain decomposition method, the mass is split into a system of two masses (m_A, m_B where $m_A + m_B = m$) and two springs (k_A, k_B where $k_A + k_B = k$) held together with an interface reaction force (Λ) (Fig. 3 [29]). On the one hand, the two masses can be integrated separately using different time steps and/or time schemes and can be coupled using the Lagrange multipliers. On the other hand, the obtained solution can be compared to a reference solution of the SDOF problem in order to plot the convergence rate with the following definition:

$$\text{Error} = \left| \frac{\mathbf{u}_{\text{subdomain}} - \mathbf{u}_{\text{reference}}}{\mathbf{u}_{\text{reference}}} \right| \tag{71}$$

One recall that the Newmark (average acceleration and central difference), Simo and Krenk time schemes are second order accurate in the linear case for transient dynamics problems [17]. In a first step, the consistency of the proposed method is studied using a calculation with the same time step for the two masses. In this respect, the convergence rate is compared to that of a single algorithm with a very fine time discretization. Then using different time scales for each mass, the time step is reduced by the same amount for each mass. In the same way, the convergence rate is also compared to that of a single algorithm. Furthermore in the case of two different time scales, a comparison between the GC and the PH method is presented. The calculation was performed through either the average acceleration scheme(A.A.), the central difference scheme (C.D.), the Simo scheme (S.) and the Krenk scheme (K.). In the proposed example, the following values are chosen: $m_A = 1.0 \times 10^{-6}$, $m_B = 1.0 \times 10^{-6}$, $k_A = 2.0 \times 10^4$ and $k_B = 3.0 \times 10^4$. The initial values are: $\mathbf{u}_A(t=0) = \mathbf{u}_B(t=0) = 1$, $\dot{\mathbf{u}}_A(t=0) = \dot{\mathbf{u}}_B(t=0) = 0$.

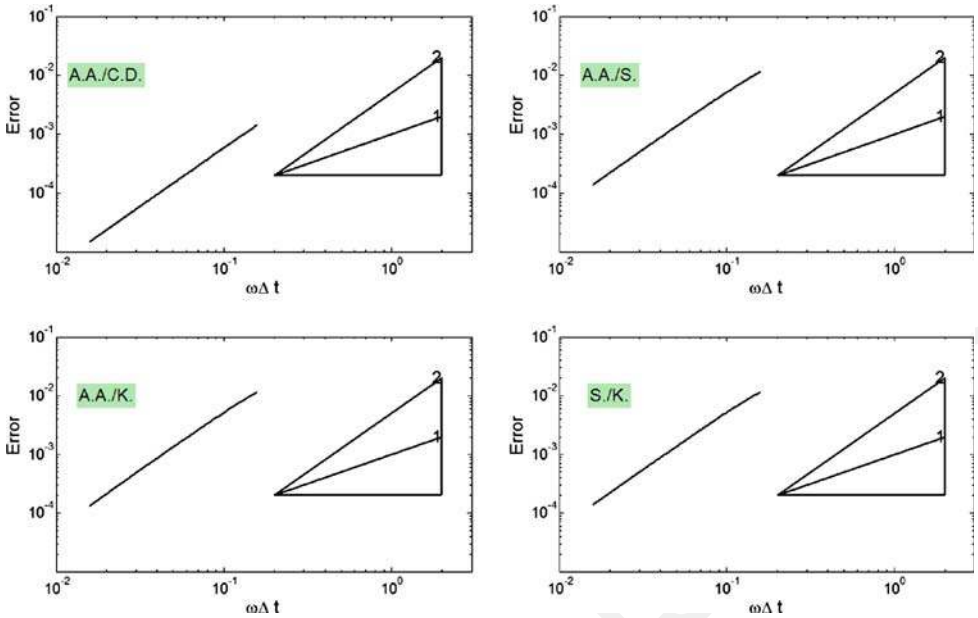

Fig. 4 Convergence rate of the GC method for a single time scale

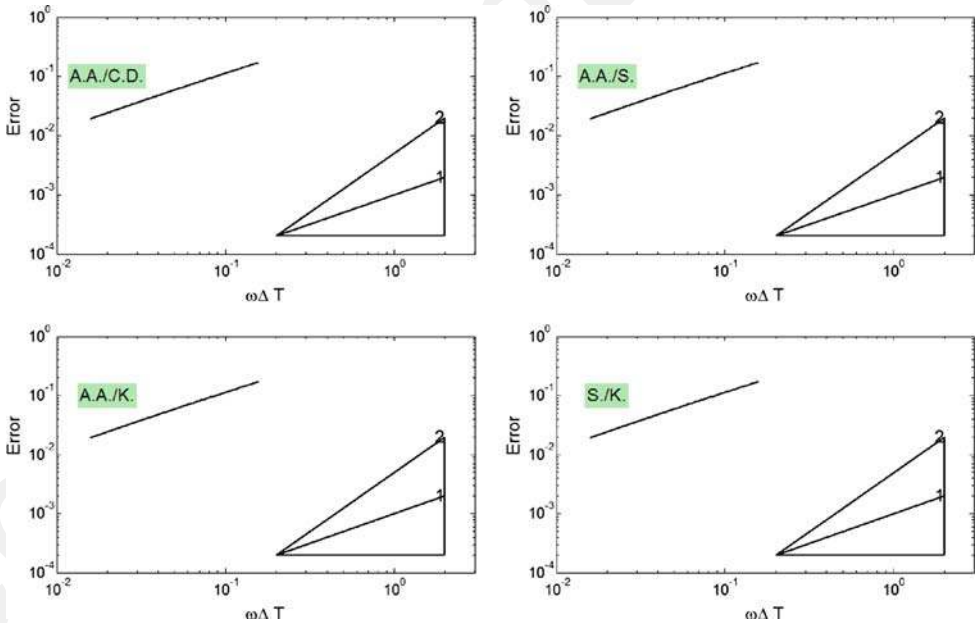

Fig. 5 Convergence rate of the GC method for different time scales: $m = 100$

3.5.1 Consistency for a single time scale problem

The same time scale is used for the two masses. The solution obtained is compared to the exact solution. With a single time scale for the two masses, the GC method is second order accurate (Fig. 4a–d) for all the considered cases (A.A/C.D.; A.A./S.; A.A./K.; S./K.). Hence, one can couple the four time schemes presented without altering the global accuracy. This method also enables the control of the accuracy locally for each subdomain in transient dynamics by the use of the most appropriate time scheme.

3.5.2 Consistency for a two time scales problem

The two masses have with their own time scale with a time scale ratio $m = 100$ ($\Delta T = m\Delta t$). In this study of the consistency, the time step is refined with the same ratio for each mass. The obtained solution is compared to the reference solution. With different time scales for the two masses, the GC method is first order accurate (Fig. 5a–d) for all the considered cases (A.A/C.D.; A.A./S.; A.A./K.; S./K.). Hence, we can see the limits of the GC method in such a case: one order of convergence rate is lost when the proposed time

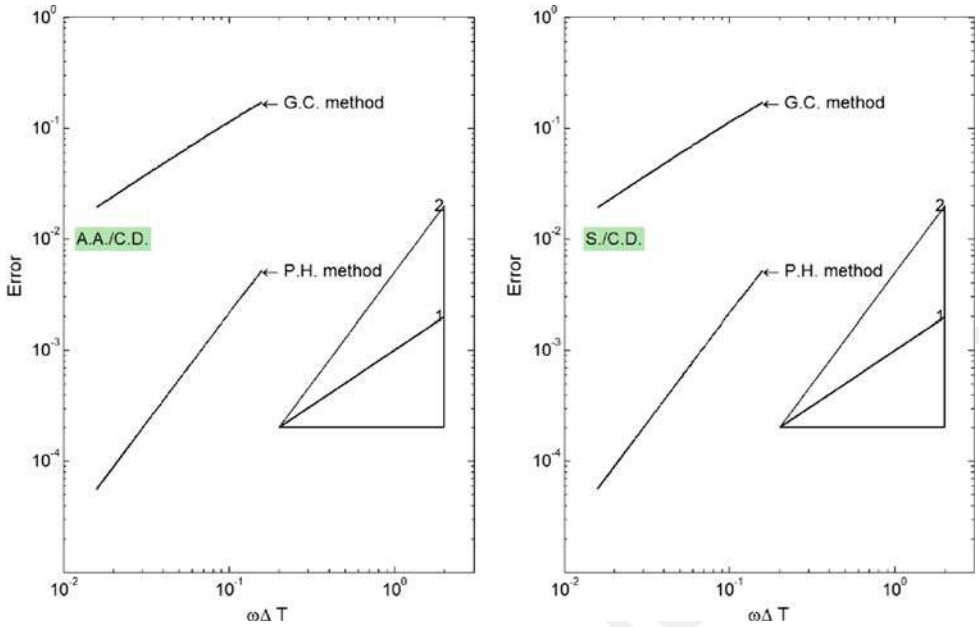

Fig. 6 Convergence rate for two time scales—comparison betwen the GC and the PH method

schemes are coupled with different time scales. Indeed, even with the use of second order accurate time schemes in each subdomain, the GC method is globally first order accurate. This limitation is clearly associated to numerical dissipation at the interface. The next proposed examples clearly illustrate this property (see Sect. 4).

3.5.3 Comparison between GC and the PH method

Here the same study is made for the PH method. The PH method is second order accurate (see Fig. 6a, b) and no numerical dissipation occurs at the interface for the considered coupling: A.A./C.D.; S./C.D; S./A.A.. Hence, the PH method is clearly an improvement of the GC method in case of different time scales. In this case, the accuracy can be controlled for each subdomain, no numerical dissipation occurs at the interface, and the global convergence rate is not altered (second order). In this respect, this result generalized the previous works of Prakash and Heljmstad (only Newmark time schemes) to a large class of numerical time schemes.

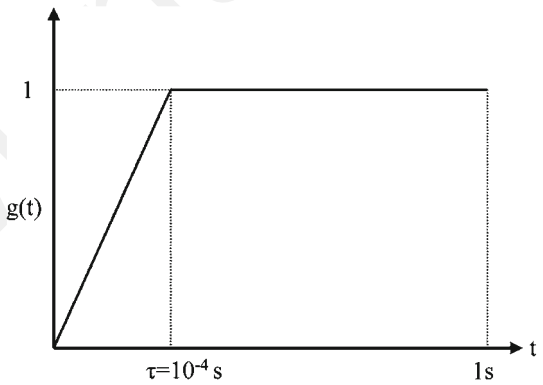

Fig. 7 Time evolution of the external load

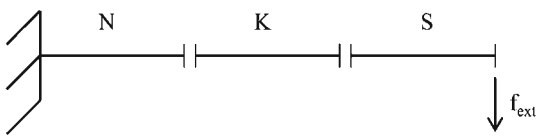

Fig. 8 Decomposition of the beam with three subdomains

4 Numerical examples

In order to validate the proposed coupling method, we propose to illustrate it through 1D, 2D (shell elments) and 3D numerical examples. One considers the numerical time schemes presented in Sect. 2. For the Newmark time schemes, we use the average acceleration implicit time scheme ($\gamma = 1/2$ and $\beta = 1/4$) and the central difference explicit time scheme ($\gamma = 1/2$ and $\beta = 0$).

4.1 1D structure with a single time scale

In this first example, we consider the case of a fixed/free beam (see Fig. 8) subjected to a bending load at the free end with the time evolution shown in Fig. 7. The aim of this example is to illustrate the ability of the proposed coupling method to mix different numerical time schemes.

A linear elastic constitutive law is assumed for the three subdomains. The material is a linear elastic isotropic and

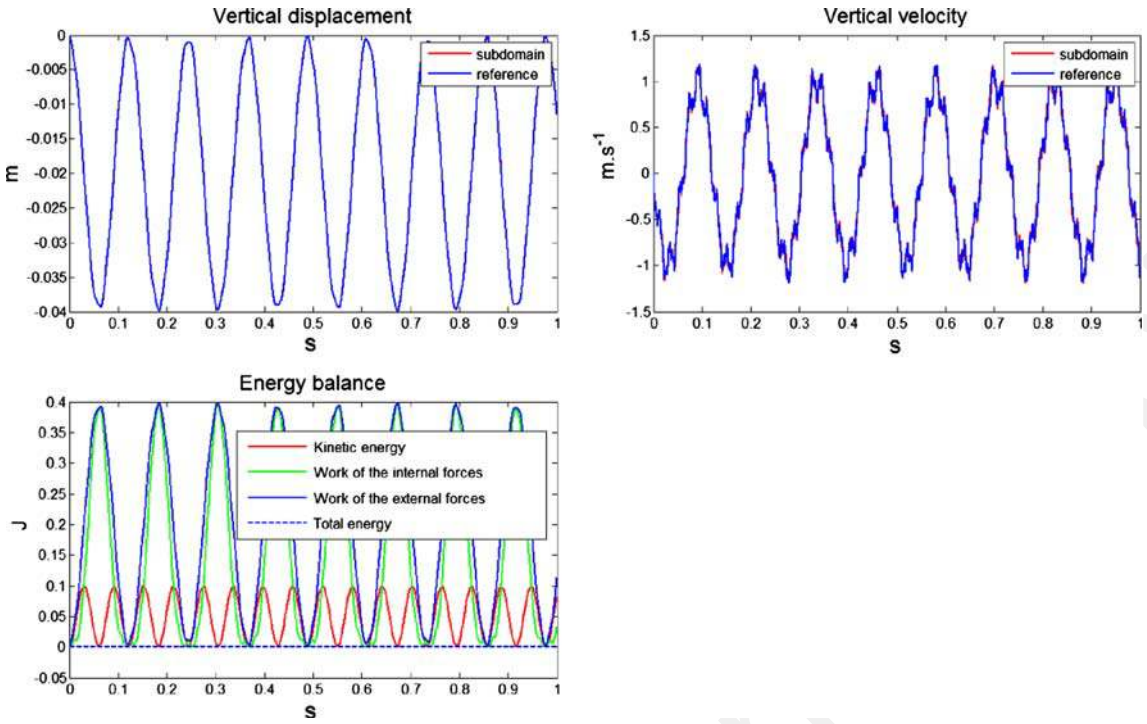

Fig. 9 Result of the 1D calculation of a beam with a bending load

homogeneous steel, with Young's modulus $E = 210 \times 10^9$ N.m^{-2}, mass density $\rho = 7{,}800$ kg.m^{-3} and Poisson's ratio $\nu = 0.3$. The structure is divided into three equal-length subdomains, and different numerical time schemes are used in each subdomain in order to calculate the global response of the beam. The length of the beam is $L = 0.9$ m with a square cross section of side $a = 0.01$ m. The beam is modeled with 2-nodes beam-type elements (six degrees of freedom per node). Thus, each of the interfaces between subdomains is a single node with six DOFs (degrees of freedom).

Figure 8 displays the 3 subdomains where N, K and S correspond to the implicit Newmark time scheme, the Krenk time scheme and the Simo time scheme respectively. This enables us to emphasize the possible numerical dissipation by such a coupling. Each subdomain is discretized with 10 beam elements. Continuity at the interface is written in terms of velocities, as presented above. In this example, the same time scale is used for the three subdomains. We plot the vertical displacement and velocity at the free end of the beam (see Fig. 9). In a second step, these results are compared to a reference calculation performed with a single-domain model and Newmark central difference time scheme. We have also performed an energy balance (see Fig. 9) in order to observe the possible numerical dissipation due to the coupling method. Indeed, the three considered time numerical schemes are second order accurate without any numerical dissipation. As consequence, the possible observed numerical dissipation is necessarily caused by the considered coupling method.

One can observe an excellent agreement of the displacements and velocities at the end of the beam between the reference calculation and the GC method (as well as for the PH method). The numerical energy balance on this example indicates no numerical dissipation induced by the coupling method. The global numerical energy balance falls within the machine tolerances, in agreement with the fact that the considered schemes involve no numerical dissipation. This example enables us to validate the proposed coupling method in the 1D linear elastic case with the same time scale for all subdomains.

4.2 2D structure with two different time scales - PH method

In this paragraph, the aim is to extend the PH method to couple different numerical time schemes in the linear case. In this respect, let us consider the problem of a beam with a traction loading (see Fig. 10) and divided into two subdomains, each with its own time scale and numerical time scheme. We arbitrarily chose the Simo scheme with a coarse time scale for the left subdomain (55 QUA4 finite elements, i.e. 66 DOFs) and the central difference scheme with a fine time scale for the right one (215 QUA4 and TRI3 finite elements, i.e. 237 DOFs). The fine time step is $\Delta t = 1.10^{-7}$ s.

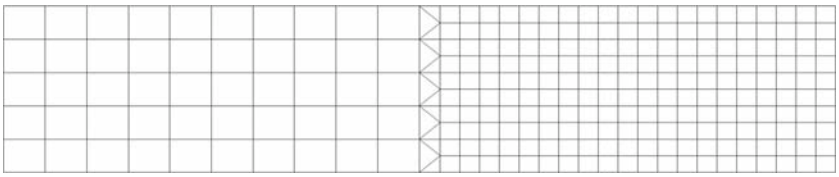

Fig. 10 Decomposition of the beam with two subdomains

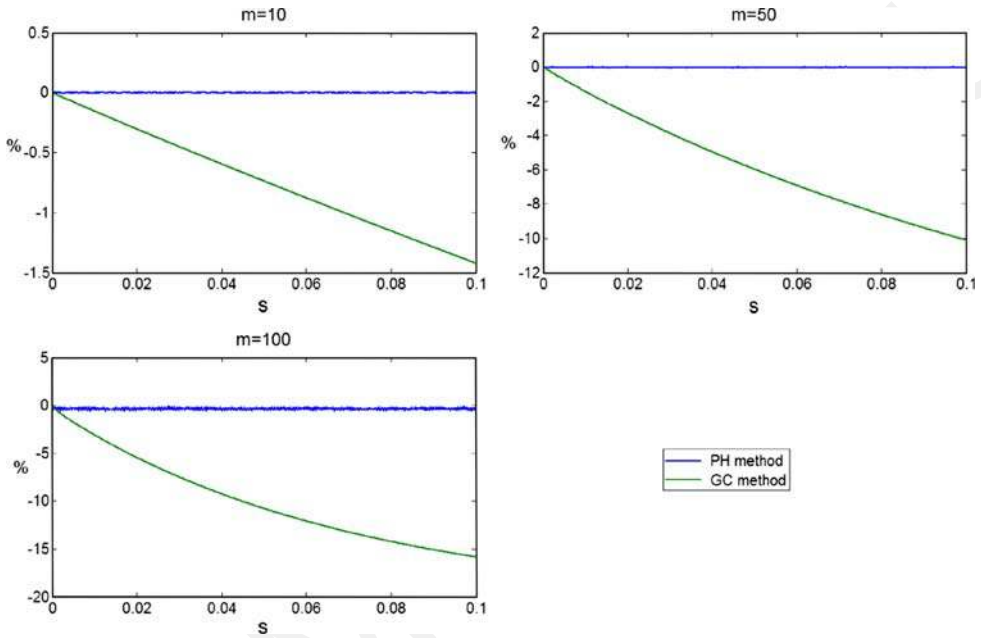

Fig. 11 Comparison of the energy balance given by the GC and the PH method

Several values of the time scale ratios m ($\Delta T = m\Delta t$): 10, 50 and 100 are considered. The material characteristics are defined as follows: Young modulus $E = 210 \times 10^9$ N.m^{-2}, mass density $\rho = 7{,}800$ kg.m^{-3} and Poisson ratio $\nu = 0.3$. The beam is clamped on its left-hand side and submitted to a step load on its right-hand side. This numerical example is an extension the use of the PH method (initially developed for Newmark schemes only) to the coupling of the average acceleration, central difference and Simo numerical schemes with different time scales. The time evolution of the loading is given in Fig. 7. Here we compare the energy balance (see Fig. 11) between the PH and the GC method for different time scale ratio in order to assess the possible numerical dissipation caused by the methods.

One can observe that the numerical dissipation of the GC method increases according to the ratio of time step but remains acceptable. However for the PH method, we observe that the energy is globally preserved for different ratios of time scale. This result is an extension of the PH method to different numerical time schemes and confirms its ability to not introducing numerical dissipation in the interface. This example illustrates the ability of the GC method and the PH method to couple different time numerical schemes with different time scales.

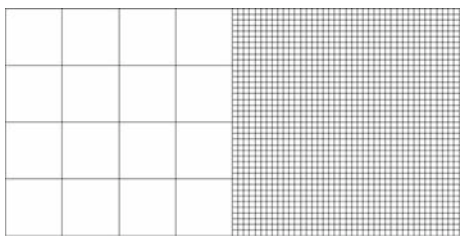

Fig. 12 Decomposition of the bar with two incompatible explicit subdomains

4.3 2D structure with two different explicit space time incompatible meshes

The aim of this section is to test the quality of the proposed method in case on explicit-explicit coupling with incompatible space and time meshes. One considers a problem of wave propagation in a homogeneous elastic bar splitted in two square domains (see Fig. 12) whose side length L is $L = 1$m. The material properties are the same as in Sect. 4.2. The two subdomains are meshed by four-nodes isoparametric quadrilateral elements in plane strain conditions. The size of the elements and time steps are ten times smaller in the fine subdomain. The coarse domain are discretized with 16

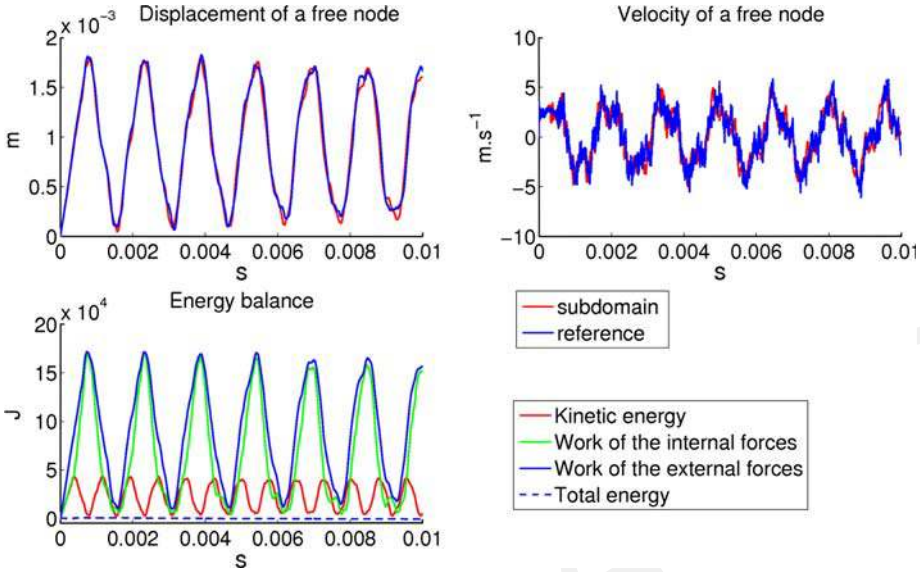

Fig. 13 Plots of time history results

QUA4 finite elements (200 DOFs) while the fine one uses 1,600 QUA4 finite elements (13,448 DOFs). Each subdomain is integrated in time by an explicit central difference scheme ($\gamma = 1/2$ and $\beta = 0$) and the time step of the finest domain is $h = 10^{-6}$ s. The left end is fixed ($u(0,\ t) = 0$) and the other end loaded by a Heaviside horizontal force $F = 10^8 N$ applied at $t = 0$ and held constant. Non-matching interfaces are used between the subdomains: hence one node of the fine mesh does not always correspond to one node of the coarse mesh. Velocities of the fine mesh nodes are enforced at each time step to follow the ones associated with the coarse one. This constraint is imposed by Lagrange multipliers and the corresponding **L** matrix. The number of Lagrange multipliers is hence equal to the number of DOFs of the fine discretisation of the interface. The simulation are uses 1,000 time steps for the coarsest time scale which is corresponds to 10,000 time step on the fine one. This allows more than six complete wave propagations along the beam. The displacement and velocity of a node of the free end of the bar are compared to a "reference" solution calculated whithout domain decomposition with a time step of $\Delta t = 2.10^{-6}$s and 1,600 QUA4 finite elements (see Fig. 13). The results are satisfactory both in amplitude and in phase. Figure 13 shows the energy balance of the method in this case. The total dissipated energy has been checked and corresponds to the work of the interface forces (within the round off errors): this is due to the dissipative nature of the GC coupling algorithm in case of non matching time steps). The numerical dissipation is less than 1% of the the work of the external loads. No numercial instability has observed on this case through the 10,000 time steps computed.

Figure 14 compares the displacements and velocities evolution for two corresponding nodes on sides A and B of the interface. The two top sub-figures compare the time histories with the "reference" solution: the results are satisfactory both in amplitude and in phase. The two lower sub-figures plot the error on velocities and displacements. The error on quantity **u** is defined as $\frac{\mathbf{u}^{\text{fine}} - \mathbf{u}^{\text{coarse}}}{\max(\mathbf{u}^{\text{fine}},\ \mathbf{u}^{\text{coarse}})}$. One may observe that the error on the velocities is within the machine tolerance (10^{-14}) and less than 1% for the displacements (see Fig. 14), but remains stable as the computation progresses.

4.4 3D structure with two time scales

The following example also deals with a fixed/free beam of length $L = 4$ m with a square cross section of dimension $a = 0.4$ m, meshed with hexaedron finite element. A bending load is applied at the free end. The structure is divided into four subdomains and a linear elastic behavior is assumed. The material consists of a steel with a Young modulus $E = 210 \times 10^9$ N.m^{-2}, a mass density $\rho = 7{,}800$ kg.m^{-3} and a Poisson ratio $\nu = 0.3$. The structure is discretized with 12,096 finite elements, i.e. 15,295 DOFs. The mesh of the four subdomains is shown in Fig. 15.

The green and blue subdomains are calculated respectively with the average acceleration and central difference Newmark time numerical schemes, while the yellow and red subdomains are calculated with the Krenk and Simo time numerical schemes respectively. On this example, one can see that some interfaces are connected to three or four subdomains. The interface betwenn the four subdomains is shown in Fig. 16.

The time evolution of the bending load is given in Fig. 7 and has a maximum value of 5.10^5 N. The time discretization of the explicit domain is chosen as the reference,

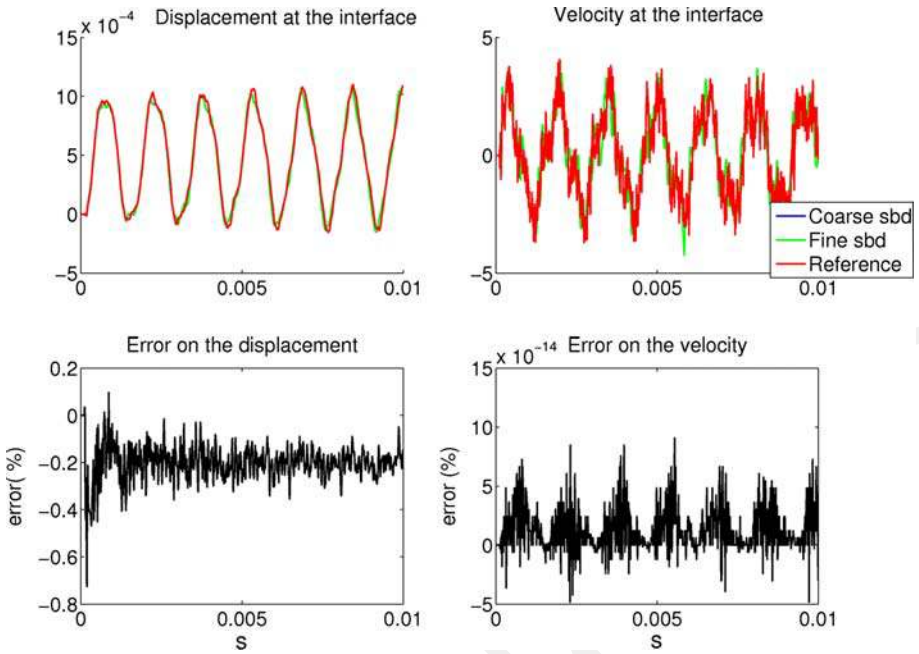

Fig. 14 Time evolution of displacement and velocities difference at interface

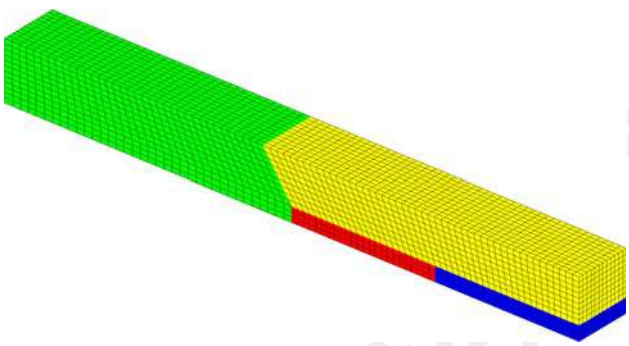

Fig. 15 The mesh of the four subdomains

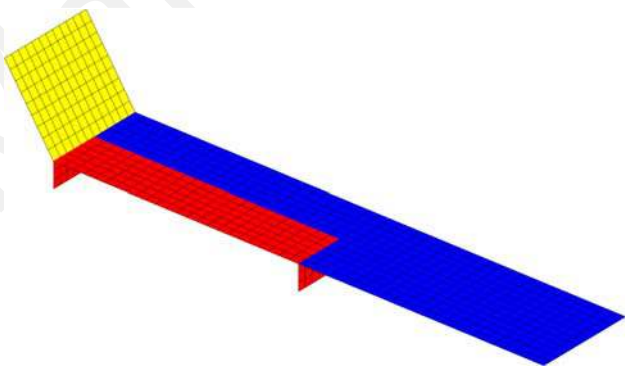

Fig. 16 The mesh of the interfaces

with the critical time step defined by the Courant condition: $\Delta t = 2.11\ 10^{-6}$ s. Several values of the time step ratio m ($\Delta T = m\Delta t$) are considered: 10, 40 and 100. Figure 17 shows, for the three time step ratios mentioned above, the vertical displacements and velocities of a point located at the free end of the beam. Finally, the third graph presents the numerical energy balances corresponding to the different values of m.

The numerical energy balances presented in Fig. 17 show the numerical dissipation which occurs when the coupling method is performed with different time scales. This numerical dissipation increases with the time step ratio. For example, the energy dissipated at the interface for $m = 100$ (400J) is 1.6% of the total energy after five periods of oscillations. This example validates the GC method to couple different time schemes and different time scales (see [10]).

4.5 3D structure with two different time scales and material nonlinearities

In this last example, we consider a pipe of length 8 m, radius 1 m and thickness 5 mm (Fig. 18). The structure is stiffened by axial and radial reinforcements, 5 mm thick and 0.1 m high. The radial stiffeners are located 1 m from the edge and 2 m from one another. The axial stiffeners are located at 90° to one another. The finite element model is built from DKT shell elements (8,664 DOFs). A vertical force with a maximum value of $-2.10^5\ N$ with the time evolution shown in Fig. 7 is applied near the right edge. The left edge is built-in.

The mesh of the structure (see Fig. 18) is divided into 6 subdomains. An exploded view of three of these subdomains is shown in Fig. 19. Four of the subdomains are calculated using implicit schemes. The red and yellow subdomains are

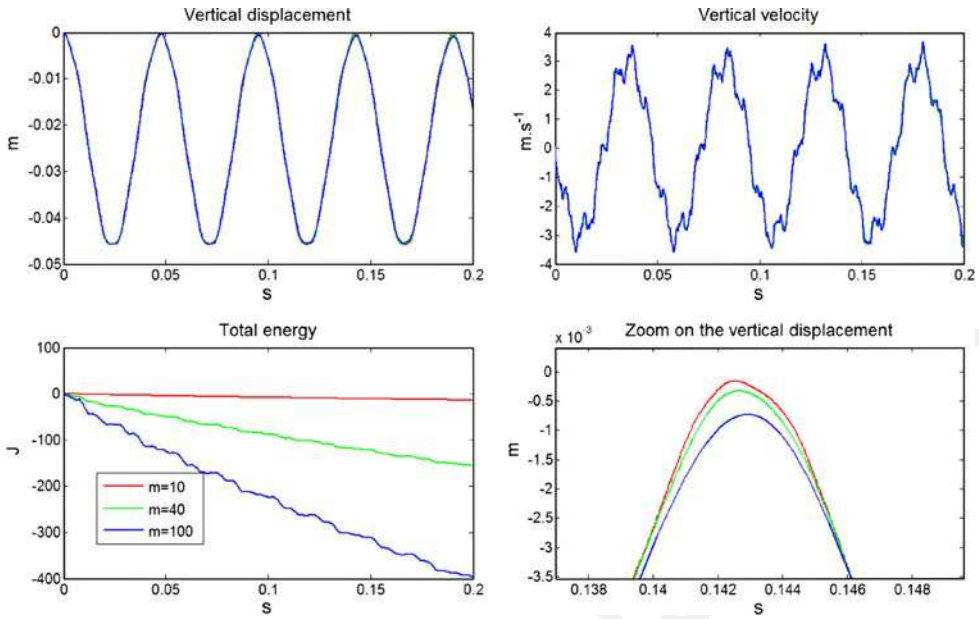

Fig. 17 Results of the 3D calculation of a beam in bending

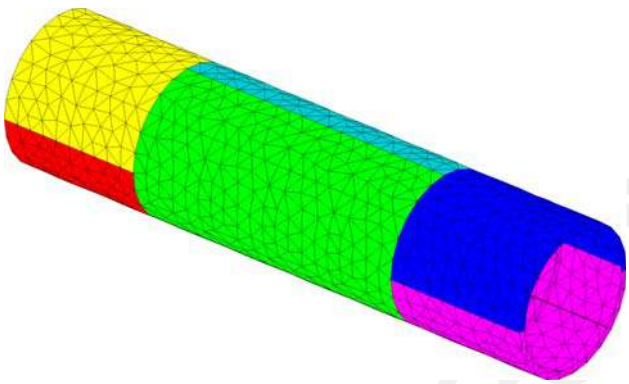

Fig. 18 The mesh of the complete structure

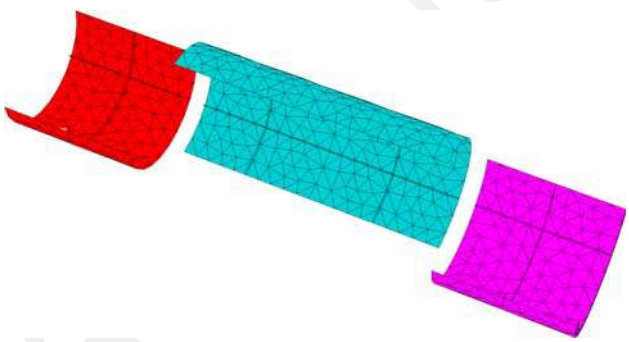

Fig. 19 Exploded view showing three of the six subdomains

calculated with the Newmark average acceleration scheme ($\gamma = 1/2$ and $\beta = 1/4$). The green and blue subdomains at the center of the structure are calculated with the midpoint scheme and the Krenk scheme respectively. A single time scale is used for the four implicit subdomains. Over these subdomains, we consider a linear elastic constitutive law with the same characteristics as in the previous examples. The remaining two subdomains, including the subdomain carrying the load, are calculated with an explicit scheme (Newmark central difference scheme $\gamma = 1/2$ and $\beta = 0$) and a different time scale than that used for the implicit subdomains. For the two "explicit" subdomains, an elastic-plastic constitutive law with isotropic strain hardening is considered. The Young's modulus, mass density and Poisson's ratio are identical to those of the previous examples. The yield stress is 200 Mpa and the tangent modulus is equal to 1% of the Young's modulus. The calculations presented below are carried out under the small displacements and small strain assumption.

We examine the displacements and velocities in the loading zone. The results obtained are compared to a reference calculation of the whole structure without subdomains, carried out using the central difference scheme ($\gamma = 1/2$ and $\beta = 0$). For this single-scale calculation, we consider an elastic-plastic constitutive law with isotropic strain hardening with the same characteristics as that used in the calculations with domain decomposition. We study two different time ratios between the two time scales ($m = 10$ and $m = 100$). Figure 20 shows the comparison of the vertical displacement and velocity from the reference calculation (blue line) with those obtained with the domain decomposition method proposed in this work using the time step ratios $m = 10$ (green line) and $m = 100$ (red line). One can observe a good agreement of the results with subdomain decomposition and those of the reference calculation, even in the case $m = 100$ with a relatively small number of steps. Furthermore, the choice of using only two subdomains with a nonlinear law rather than the whole structure (as in the reference calcula-

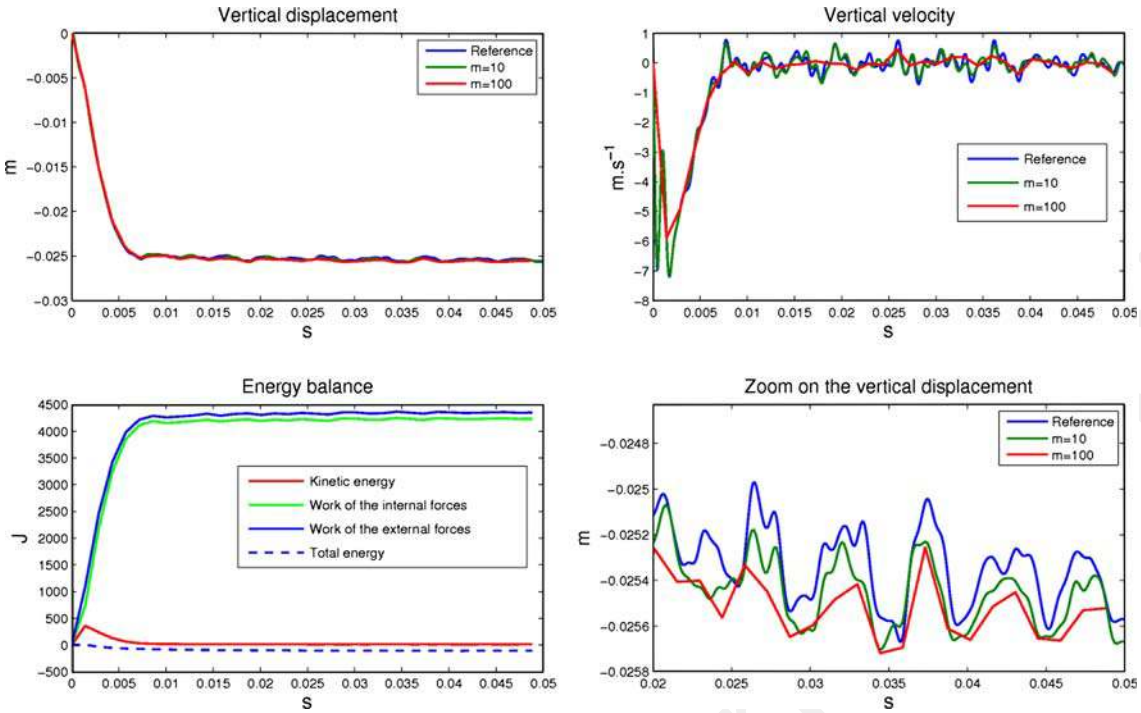

Fig. 20 Results of the 3D analysis of a pipe with axial and radial stiffeners

tion) appears justified by the results. The energy balance presented in Fig. 20 is obtained with the time step ratio $m = 100$. In this case, the numerical dissipation of the interface forces is 2.5% of the total energy.

5 Conclusion

In this article, one proposes a general formalism which enables the coupling of a wide range of numerical time schemes (Newmark, Simo, Krenk). The Krenk numerical time scheme is introduced with the Lagrange multipliers in order to use it in a domain decomposition method within a dual Schur type formalism. Single and multi-time-scale numerical examples with linear elastic as well as nonlinear elasto-plastic laws were presented in order to illustrate the robustness and accuracy of the proposed GC coupling method. Generally speaking, this approach can be implemented into industrial codes without major modification of their existing architectures. This will give the user of such a code access to numerical methods for nonlinear transient dynamics and offers the possibility to choose, subdomain by subdomain, the adapted numerical time scheme and the most suitable time scale. This methodology can also be extended to the coupling of codes with different time integration schemes. Furthermore, this requires carrying out a global energy balance during the resolution in order to control the possible numerical dissipation between subdomains. One can also extend the presented approach to the PH method in order to achieve zero numerical dissipation at the interface. In this paper, the PH method has been extended to the coupling of Newmark and Simo numerical time schemes with different time scales. In the continuation of this work, it can be interesting to extend the PH approach both for other time schemes and transient non linear dynamic problems.

Acknowledgments The authors wish to acknowledge EDF, Direction Recherche et Développement (AMA/T62) at Clamart (France) for its financial support.

References

1. Belytschko T, Mullen R (1976) Mesh partitions of explicit-implicit time integration In: Proceedings US–Germany symposium on formulations and computationnal algoritms in finite element analysis
2. Belytschko T, Mullen R (1978) Stability of explicit-implicit mesh partitions in time integration. Int J Numer Methods Eng 12:1575–1586
3. Liu WK, Belytschko T (1982) Mixed-time implicit-explicit finite elements for transient analysis. Comput Struct 15:445–450
4. Liu WK, Belytschko T, Zhang YF (1984) Implementation and accuracy of mixed-time implicit-explicit methods for structural dynamics. Comput Struct 19:521–530
5. Belytschko T, Liu WK, Smolinski P (1987) Stability of multi-time step partitioned transient analysis for first-order systems of equation. Comput Methods Appl Mech Eng 65:115–125
6. Ben Dhia H. (1998) Multiscale mechanical problems: the Arlequin method. Comptes Rendus de l'Académie des Sci Ser IIB Mech Phys Astron 12:899–904

7. Bourel B (2006) Calcul multi-domaines et approches multi-échelles pour la simulation de crashs automobiles, Thèse de doctorat. Institut National des Sciences Appliquées de Lyon
8. Bourel B, Combescure A, Valentin LD (2006) Handling contact in multi-domain simulation of automobile crashes. Finite Elements Analy Des 42:766–779
9. Cavin P, Gravouil AA, Combescure A (2005) Automatic energy conserving space-time refinement for linear dynamic structural problems. Int J Numer Methods Eng 50:304–321
10. Combescure A, Gravouil A (2002) A numerical scheme to couple subdomains with different time-steps for predominantly linear transient analysis. Comput Methods Appl Mech Eng 191:1129–1157
11. Daniel WJT (1998) A study of the stability of subcycling algorithms in structural dynamics. Comput Methods Appl Mech Eng 156:1–13
12. Dodds JRH, Lopez LA (1980) Substructuring in linear and nonlinear analysis. Int J Numer Methods Eng 15:583–597
13. Farhat C, Roux F-X (1991) A method of finite element tearing and interconnecting and its parallel solution algorithm. Int J Numer Methods Eng 32:1205–1227
14. Farhat C, Crivelli L, Geradin M (1993) On the spectral stability of time integration algorithms for a class of constrained dynamics problems. In: Collection of technical papers AIAA/ASME structures, structural dynamics and materials conference. AIAA: Washington DC, USA, pp 80–97
15. Farhat C, Crivelli L, Roux F-X (1994) Transient FETI methodology for large-scale parallel implicit computations in structural mechanics. Int J Numer Methods Eng 37:1945–1975
16. Faucher V, Combescure A (2004) Local modal reduction in explicit dynamics with domain decomposition. Part 1: extension to subdomains undergoing finite rigid rotations. Int J Numer Methods Eng 60:2531–2560
17. Gérardin M, Rixen D (1996) Théorie des vibrations—application à la dynamique des structures (2ème édition). Masson Editions, Paris
18. Glowinski R, Le Tallec P (1990) Augmented lagrangian interpretation of the non-overlapping schwarz alternating method In: Domain decomposition method. SIAM, Philadelphia, pp 224–231
19. Gravouil A (2000) Méthode multi-échelles en temps et en espace avec décomposition de domaines pour la dynamique non linéaire des structures. Thèse de doctorat. Ecole Normale Supérieure de Cachan
20. Gravouil A, Combescure A (2001) A multi-time-step explicit-implicit method for non-linear structural dynamics. Int J Numer Methods Eng 50:199–225
21. Herry B (2002) Développement dune approche multiéchelle parallèle pour la simulation de crash automobile non linéaire des structures. Thèse de doctorat. Ecole Normale Supérieure de Cachan
22. Herry B, Di Valentin L, Combescure A (2002) An approach to the connection between subdomains with non-matching meshes for transient mechanical analysis. Int J Numer Methods Eng 55:973–1003
23. Hughes TJR, Liu WK (1978) Implicit-Explicit finite elements in transient analysis: stability theory. ASME J Appl Mech 45:371–374
24. Hughes TJR, Liu WK (1978) Implicit-Explicit finite elements in transient analysis: implementation and numerical examples. ASME J Appl Mech 45:375–378
25. Joly P, Rodrìguez J (2005) An error analysis of conservative space-time mesh refinement methods for the 1D wave equation. SIAM J Numer Anal 43:825–859
26. Krenk S (2007) Energy conservation and high-frequency damping in numerical time integration. In: Computational Methods in Structural Dynamics and Earthquake Engineering; Rethymno, Crete, Greece, 12
27. Magoules F, Roux FX (2006) Lagrangian formulation of domain decomposition methods: a unified theory. Appl Math Model 30:593–615
28. Newmark NM (1959) A method of computation for structural dynamics. J Eng Mech Div ASCE 85:67–94
29. Prakash A, Hjelmstad KD (2004) A FETI-based multi-time-step coupling method for Newmark schemes in structural dynamics. Int J Numer Methods Eng 61:2183–2204
30. Schwarz HA (1870) Über einen Grenzübergang durch alternierendes Verfahren. Vierteljahrssch der Naturforsch Ges Zür 15:272–286
31. Simo JC, Wong KK (1991) Unconditionally stable algorithms for rigid body dynamics that exactly preserve energy and momentum. Int J Numer Methods Eng 31:19–52